

**OPEN ACCESS**

# Sulfonic Acid Based Complex Framework Materials (CFM): Nanostructured Polysulfide Immobilization Systems for Rechargeable Lithium–Sulfur Battery

To cite this article: Pavithra M. Shanthy *et al* 2019 *J. Electrochem. Soc.* **166** A1827

View the [article online](#) for updates and enhancements.



**PRIME**<sup>TM</sup>  
PACIFIC RIM MEETING  
ON ELECTROCHEMICAL  
AND SOLID STATE SCIENCE  
**2020**

*Abstract Submission*  
**DEADLINE EXTENDED:**  
*May 29, 2020*

**Honolulu, HI | October 4-9, 2020**





## Sulfonic Acid Based Complex Framework Materials (CFM): Nanostructured Polysulfide Immobilization Systems for Rechargeable Lithium–Sulfur Battery

Pavithra M. Shanthi,<sup>1</sup> Prashanth J Hanumantha,<sup>2</sup> Kuruba Ramalinga,<sup>2</sup> Bharat Gattu,<sup>1,\*</sup> Moni K Datta,<sup>2,3,4</sup> and Prashant N. Kumta<sup>1,2,3,4,5,\*\*,z</sup>

<sup>1</sup>Department of Chemical and Petroleum Engineering, University of Pittsburgh, Pittsburgh, Pennsylvania 15261, USA

<sup>2</sup>Department of Bioengineering, University of Pittsburgh, Pittsburgh, Pennsylvania 15261, USA

<sup>3</sup>Center for Energy, University of Pittsburgh, Pittsburgh, Pennsylvania 15261, USA

<sup>4</sup>Center for Complex Engineered Multifunctional Materials, University of Pittsburgh, Pittsburgh, Pennsylvania 15261, USA

<sup>5</sup>Department of Mechanical Engineering and Materials Science, University of Pittsburgh, Pittsburgh, Pennsylvania 15261, USA

Lithium-sulfur (Li-S) secondary batteries with sulfur cathodes and theoretical energy density of ~2600 Wh/kg, are promising high energy-density system for next-generation electric-vehicles (EVs) potentially mitigating the gravimetric and volumetric energy density limitations of existing lithium-ion (Li-ion) batteries. Herein, a chemically synthesized sulfonic acid-based complex framework material (CFM) termed as (SCFM), was used as sulfur host (S-SCFM) to prevent polysulfide dissolution in Li-S batteries. The S-SCFM based CFM cathodes show an initial capacity of 1190 mAh/g and a capacity of 1044 mAh/g after 100 cycles. In addition, the S-SCFM based CFM cathodes exhibited good cycling stability with a minimal fade rate of ~0.0012% per cycle. XPS analysis of the cycled separators with the S-SCFM electrodes shows complete absence of polysulfide species after 100 charge-discharge cycles. It was also identified that the SCFM based CFM chemically binds sulfur via -C-S- linkages thereby exhibiting an affinity for the polysulfide species formed during the charge-discharge cycles. As a result, the SCFM based CFM prevent polysulfide species from dissolving and diffusing into the electrolyte. A thorough understanding of these engineered SCFM based CFM sulfur host in Li-S battery outlined herein will be vital in designing promising sulfur hosts for next generation sulfur cathodes in Li-S batteries.

© The Author(s) 2019. Published by ECS. This is an open access article distributed under the terms of the Creative Commons Attribution 4.0 License (CC BY, <http://creativecommons.org/licenses/by/4.0/>), which permits unrestricted reuse of the work in any medium, provided the original work is properly cited. [DOI: 10.1149/2.0251910jes]



Manuscript received April 22, 2019. Published June 4, 2019.

The rapid evolution of electric vehicles, combined with the emergence of large scale stationary and portable electronic devices has given rise to an urgent demand for rechargeable batteries with high energy densities and long cycle life at low cost.<sup>1,2</sup> Owing to their high volumetric<sup>3</sup> and gravimetric energy densities,<sup>4</sup> lithium-ion (Li-ion) batteries are the principal power sources in portable electronic devices such as cell phones and laptops.<sup>5</sup> However, the energy density (80–170 Wh/kg) and power density (800–200 W/kg)<sup>6</sup> of currently available rechargeable Li-ion batteries are inferior, requiring significant improvements in gravimetric and volumetric energy and power densities, with adequate cost match to power electric vehicles in order to meet the DOE target of \$125/kWh by 2020.<sup>7</sup> Despite much improvement since the commercialization of the Li-ion battery in 1991, the specific capacities of most commonly used layered oxide-based cathodes LiMO<sub>2</sub>, M = Ni, Co, Mn (~150 mAh/g)<sup>8</sup> and M = Fe (~170 mAh/g)<sup>9</sup> are significantly lower than those of graphite (370mAh/g)<sup>10</sup> and silicon (~4200 mAh/g)<sup>11</sup> anodes. It is therefore, extremely important to develop new cost-effective cathode and anode chemistries for rechargeable Li-ion batteries.

Among different lithium battery cathodes explored, sulfur exhibits a theoretical capacity of 1672 mAh/g,<sup>12</sup> significantly higher than hitherto insertion-based cathode materials. Lithium-Sulfur (Li-S) batteries operate via a two-electron reaction pathway, presenting exceptionally high theoretical energy densities of 2600 Wh/kg.<sup>13</sup> In addition to the high energy and power densities, sulfur exhibits other advantages. These include low cost (\$100/kWh of Li-S batteries comprising lithium metal anode and sulfur cathode)<sup>14</sup> compared to conventional cathodes (\$432/kWh graphite anode and lithium nickel magnesium cobalt oxide (NMC) cathode),<sup>14,15</sup> natural abundance (0.07% of the Earth's crust),<sup>16</sup> and environmental friendliness. Thus, Li-S batteries can be established as a promising candidate to satisfy the extensive requirements of the electric vehicle (EV) technologies as well as other consumer portable and electronic devices related energy storage market.

However, the insulating nature of sulfur results in low active material utilization.<sup>17</sup> Furthermore, conversion of sulfur to Li<sub>2</sub>S causes a large volume expansion (~80%).<sup>18</sup> More importantly, the reaction of sulfur with lithium leads to the formation of polysulfide intermediates (S<sub>n</sub><sup>2-</sup>, 3 ≤ n ≤ 8)<sup>19</sup> that are highly soluble in organic battery electrolytes, resulting in loss of energy-bearing active materials yielding poor cycling stability. Polysulfide dissolution also causes a change in the electrolyte composition during cycling and its impact on the solid electrolyte interphase (SEI),<sup>19–21</sup> a major contributor to performance decay, additionally being poorly understood. These challenges have hindered the commercial progression of Li-S batteries for practical applications.

In order to address the obstacles facing Li-S batteries, extensive research is being conducted in recent years. These include designing composite nanostructured architectures to immobilize the sulfur and polysulfides within the cathode,<sup>22–26</sup> thus increasing the active material utilization and controlling polysulfide dissolution. Introducing a carbon interlayer between the cathode and the separator<sup>27–29</sup> has helped contain the polysulfides within the cathode serving as an extended current collector. Furthermore, solid, composite, and gel polymer electrolytes have also been used to block polysulfide dissolution, diffusion, and migration. The addition of LiNO<sub>3</sub> as an electrolyte additive<sup>30–32</sup> to promote the formation of a passivation film at the lithium/electrolyte interface has also proven to be effective in preventing polysulfide dissolution. Additionally various nano-sized metal oxides, such as manganese nickel oxide,<sup>33</sup> γ-alumina,<sup>34</sup> silica,<sup>35</sup> and titania<sup>21</sup> have shown to improve the Li-S battery performance by absorbing and trapping the soluble polysulfides.

Amongst all the reported approaches, the most popular method documented is the employment of nanoporous carbon hosts to improve the Li-S battery performance<sup>13,24,36,37</sup> while ensuring that the sulfur particles are nano-sized with the ability to encapsulate sulfur and polysulfides within their pores during cycling. Numerous porous carbonaceous materials have been used as sulfur hosts, including microporous and mesoporous carbons,<sup>22–26,38–42</sup> porous carbon spheres,<sup>26</sup> activated carbon fibers,<sup>43</sup> carbon nanotubes<sup>44</sup> and graphene nanosheets.<sup>45</sup> All these approaches have had a positive impact on the cycling stability of Li-S batteries.

\*Electrochemical Society Student Member.

\*\*Electrochemical Society Member.

<sup>z</sup>E-mail: [pkumta@pitt.edu](mailto:pkumta@pitt.edu)

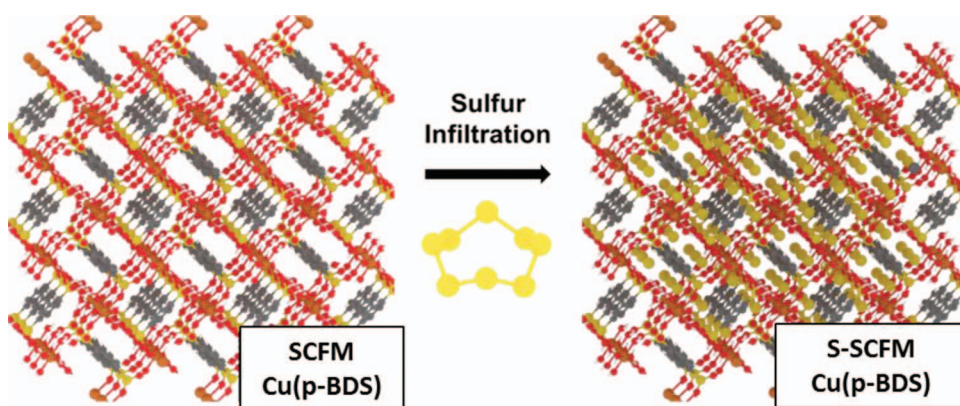


**Figure 1.** Schematic representation of the CFM derived SCFM before and following sulfur infiltration.

In general, carbon hosts confine sulfur and polysulfides within the pores or interlayers by physically interacting with the sulfur. The weak physical interaction however, can only retain polysulfides partially and for only a short period. Consequently, the dissolved polysulfides will eventually diffuse out of the cathode during the charge-discharge processes. Recently, it has been proven that the use of metal oxides,<sup>46,47</sup> metal sulfides<sup>48,49</sup> and metal organic frameworks (MOFs)<sup>50–52</sup> immobilize polysulfide species by chemical adsorption. MOFs are a new class of crystalline porous materials made of metal ions or cluster nodes linked by organic ligands in infinite arrays. MOFs are also easy to design with the ability to add various chemical moieties on the surface for further functionalizing the system with potential applications in gas storage, separations, catalysis, detection, and electrochemistry. In recent years, the use of MOFs as hosts for immobilizing sulfur in Li-S batteries has also attracted much interest.<sup>53–55</sup> Metal nodes within the MOF form Lewis acid sites, and the functional groups from the organic linkers form Lewis base sites, together with the nanoporous architecture providing effective binding sites for the lithium polysulfides<sup>56</sup> and hence, strongly confining them within the pores. The nanoporous framework also offers a platform for researchers to design materials for effectively restraining the dissolution and diffusion of polysulfides at the molecular level.

Until now, most reports on MOFs for Li-S batteries exploited the pore size of carbonized MOFs to limit the polysulfide dissolution.<sup>53,55,57–60</sup> Only few reports reflect the use of Lewis acid and Lewis base sites within the MOFs to serve as active binding sites for polysulfide dissolution;<sup>51,52,54,56,61</sup> noteworthy being Wang et al.<sup>61</sup> and Zheng et al.<sup>56</sup> reporting on carbonate-based MOFs used as sulfur hosts for Li-S batteries. It is important to note that there is a significant initial loss in capacity in both reports with no adequate scientific explanation. We have previously reported extensively on the reason for the observed irreversible loss in capacity in carbonate based MOFs used in Li-S batteries.<sup>50</sup> The observed loss in irreversible capacity in carbonate-based MOFs is attributed to the reaction of sulfur with the carbonate functional groups of the MOFs during cycling. With this understanding, putatively using a sulfonic acid functionalized MOF as a sulfur host forming a complex framework material (CFM) could essentially mitigate this observed initial capacity loss.

In this work, accordingly, we report on the use of a novel complex framework material (CFM) based CFM synthesized from sulfonic acid analogues of carboxylic acid, reported by Mietrach et al.,<sup>62</sup> as sulfur hosts for Li-S batteries. A simple room temperature method was used to synthesize the sulfonic acid-based CFM termed SCFM, followed by infiltration of sulfur using a vapor phase infiltration process before using it as cathode in Li-S batteries. (Figure 1). The sulfur infiltrated CFM termed S-SCFM cathodes, when tested in Li-S battery shows an initial capacity of 1190 mAh g<sup>-1</sup> with a stable capacity of at 1044 mAh g<sup>-1</sup> for over 100 cycles. In addition, these cathodes exhibit a total prevention of polysulfide dissolution along with negligible fade rate (0.0014% cycle<sup>-1</sup>) (evident from XPS analysis and electrochemical

cycling testing, respectively) making these cathode systems promising candidates for Li-S batteries. X-ray photoelectron spectroscopy (XPS) was subsequently used to further understand the S-C bonding characteristics and provide additional insights into the prevention of polysulfide dissolution. Results of these studies are accordingly described in detail in the following sections.

## Experimental

### Preparation of sulfonic acid CFMs and sulfur infiltration.—

Benzene-1,4-dithiol (99% (GC)), hydrogen peroxide solution (30 wt% in H<sub>2</sub>O, ACS reagent), methanol (>99.8%, ACS reagent), copper (II) carbonate (basic, ACS reagent) and sulfur (325 mesh particle size, ACS reagent) were purchased from Sigma-Aldrich and used without any further treatment or purification.

1,4-benzenedisulfonic acid dihydrate (p-BDSH<sub>2</sub>·2H<sub>2</sub>O) was prepared by dissolving 9.0mM (1.3g) 1,4-benzene dithiol in warm methanol (18ml) and H<sub>2</sub>O<sub>2</sub> (15ml) as reported by Mietrach et al.<sup>62</sup> The suspension was stirred for 16 h at 25°C. All volatile materials were then removed under high vacuum to yield a colorless solid of (p-BDSH<sub>2</sub>·2H<sub>2</sub>O).

Copper(II) (1,4-benzenedisulfonate) tetrahydrate [Cu(p-BDS) - (H<sub>2</sub>O)<sub>4</sub>/Sulfonic - CFM/SCFM] was prepared by mixing copper II carbonate (40 mg) and 1,4-benzenedisulfonic acid (0.1 g) in 5 ml water and heating at 50°C under stirring for one day as reported by Mietrach et al.<sup>62</sup> The resulting solution was then filtered and after a few days in air at room temperature in a small petri dish, blue crystals of Cu(p-BDS) - (H<sub>2</sub>O)<sub>4</sub> were obtained from the blue solution.

The CFM derived SCFM was infiltrated with sulfur<sup>63</sup> under vacuum. The sulfur weight to be infiltrated into the CFM derived SCFM was calculated from the pore volume of the SCFM (70:30 wt% S: SCFM) and was accordingly sealed in a quartz ampoule under vacuum. The ampoule was then heated at 300°C for 24 h to impregnate sulfur into the CFM derived SCFM to obtain the sulfur infiltrated-SCFM, referred as (S-SCFM) henceforth in this manuscript.<sup>50</sup>

**Chemical and electrochemical characterization.**—X-Ray diffractometry (XRD) was used to characterize the SCFM using a Philips XPERT Pro X-Ray diffractometer. The diffractometer employs CuK<sub>α</sub> radiation with a wavelength of 0.15406 nm to record the 2θ scans in the 10–50° range. The current and voltage were set constant at 40 mA and 45 kV, respectively during the measurements. High-Resolution Transmission Electron Microscopy (HRTEM) imaging of the CFM derived SCFM and S-SCFM was performed using a JEOL JEM2100F equipment to derive a better understanding of the morphology.

X-Ray Photoelectron Spectroscopy (XPS) analysis of the CFM derived SCFM and S-SCFM was performed in an ESCALAB 250 Xi system employing Al K<sub>α</sub> as the X-Ray source. A sample spot of 200 × 200 μm<sup>2</sup> was defined for XPS analysis under uniform charge

**Table I. Results of BET analysis of SCFM and S-SCFM. (Each datum represents an average of three independent tests run on three different samples prepared under identical conditions.)**

	BET Surface Area (m <sup>2</sup> /g)	Langmuir Surface Area (m <sup>2</sup> g <sup>-1</sup> )	Total Pore Volume (cm <sup>3</sup> g <sup>-1</sup> )	Adsorption average pore width (nm)
SCFM	266.4 ± 17.84	452.6 ± 21.54	0.623 ± 0.07	3.2 ± 0.12
S-SCFM	7.60 ± 1.42	12.36 ± 0.94	0.0018 ± 0.0002	11.19 ± 0.44

neutralization conditions established using a beam of Ar<sup>+</sup> ions and enactors guided using magnetic lens. The XPS measurements were performed under a pressure of <math>5 \times 10^{-10}</math> mbar. The analyzer was calibrated to provide <math><50</math> meV deviation in binding energy of Au 4f<sub>7/2</sub> (83.98 eV), Ag 3d<sub>5/2</sub> (368.26 eV) and Cu 2p<sub>3/2</sub> (932.67 eV). The data collected from the spectrometer was analyzed using the Advantage software package.

A Micromeritics ASAP 2020 analyzer was used to analyze the specific surface area and pore characteristics of the CFM samples. The Brunauer–Emmett–Teller (BET) isotherms were obtained after vacuum degassing followed by conducting nitrogen adsorption-desorption experiments on the samples.

The cathodes for electrochemical charge-discharge cycling evaluation were prepared by coating a homogeneous slurry of the CFM derived S-SCFM (80 wt%), super P (10 wt%) and polyvinylidene fluoride (PVdF) (10 wt%) dispersed in N-methyl pyrrolidone (NMP) onto an aluminum foil (MTI corporation). The slurry coated foils were then dried under ambient conditions for 24 hours. The loading of the slurry coated electrodes was maintained uniformly at 1.5–2 mg cm<sup>-2</sup>. Commercial sulfur (Sigma Aldrich, Inc, 99%) was also used to generate the control electrodes of identical composition to compare the electrochemical performance of the S-SCFM.

The sulfur infiltrated sulfonic acid derived CFM termed S-SCFM cathodes (working electrode) were assembled into 2025-coin cells in a glove box under Argon (H<sub>2</sub>O <math><0.1</math> ppm, O<sub>2</sub> <math><0.1</math> ppm). The coin cells contained lithium metal counter electrode using a Celgard polypropylene (PP) separator and 1.8 M LiCF<sub>3</sub>SO<sub>3</sub> (lithium trifluoromethanesulfonate) + 0.2 M LiNO<sub>3</sub> in 50:50 vol% 1, 3 dioxolane and 1, 2 dimethoxyethane electrolyte. The coin cells were tested in an Arbin BT200 battery tester between 1.7-2.6 V (w.r.t. Li<sup>+</sup>/Li) at 0.1 C current rate. Cyclic Voltammetry (CV) and Electrochemical Impedance Spectroscopy (EIS) experiments on the batteries were performed using a VersaSTAT (Princeton Applied Research) potentiostat. The CV experiments were carried out employing a scan rate of 0.1 mVs<sup>-1</sup> between 1.7 V-2.6V. The impedance spectra were performed by varying the frequency between 100 kHz and 10 mHz at an amplitude of 10 mV w.r.t the open circuit potential. The obtained EIS data were then fitted using the ZView software (Scribner and Associates).

## Results and Discussion

The crystal structure of the CFM derived SCFM was studied using XRD. Experimentally obtained XRD patterns of the SCFM was compared with the corresponding pattern simulated using the crystallographic information file (CIF) of the SCFM<sup>62</sup> obtained from the Cambridge Crystallographic Data Centre (via [www.ccdc.cam.ac.uk/data\\_request/cif](http://www.ccdc.cam.ac.uk/data_request/cif)) (CCDC number 738978) to ascertain the phase-purity of the synthesized SCFM. Figure 2 represents a comparison of the XRD patterns of the experimentally obtained SCFM against the simulated pattern for the corresponding SCFM. A good fit between the simulated and the experimentally obtained XRD patterns implies that the SCFM<sup>62</sup> is phase pure and indeed crystalline in nature.

Pore size and pore volume of the experimentally synthesized SCFM is a critical factor in determining the amount of sulfur that can be completely infiltrated into the SCFM structure. The porosity of the experimentally synthesized SCFM and S-SCFM were accordingly analyzed using BET and the results of the pore size and surface area analysis are shown in Table I (Figure S1 shows the corresponding adsorption isotherms). The experimentally obtained SCFM structure exhibits a

specific surface area (SSA) of  $\sim 452.6$  m<sup>2</sup>g<sup>-1</sup>, an average pore size of  $\sim 3.2$  nm and a pore volume of  $\sim 0.623$  cm<sup>3</sup>g<sup>-1</sup>. The experimentally determined specific surface area values are comparable with the specific surface area corresponding to conventional CFMs or MOFs studied and reported for gas storage and energy storage applications for Li–S batteries.<sup>40,41,64–68</sup> The small average pore diameter of the SCFM ( $\sim 3.2$  nm) is expected to aid in preventing polysulfide dissolution by facilitating improved trapping of the polysulfides formed during electrochemical cycling. The sulfur infiltrated CFM derived S-SCFM, on the other hand, shows a drastic reduction in surface area (12.36 m<sup>2</sup>g<sup>-1</sup>) which is clearly indicative of the pores being filled by sulfur and is thus, attributed to sulfur infiltration into the porous channels of the chemically derived CFM based SCFM which results in filling up of the pores. Pore closure in CFMs upon interaction with other molecules similar to sulfur herein is a well-studied phenomenon and our results are thus consistent with reports in the literature.<sup>69,70</sup>

TEM analysis was subsequently performed on the experimentally synthesized SCFM to confirm the nanoporous nature and on the sulfur infiltrated CFM structures, namely, S-SCFM to confirm that the infiltrated sulfur had indeed entered and occupied the pores within the experimentally generated SCFM structure (Figures 3a–3d). The HR-TEM image of the CFM derived S-SCFM at low magnification shows the microscopic structure of the SCFM and the high-resolution image (Figure 3b) further shows the highly ordered nature of the SCFM while the corresponding SAED (Selected Area Electron Diffraction) pattern of the SCFM (inset Figure 3b) indicates the expected long-range order of the SCFM channels. Figure 3c represents the corresponding HR-TEM image of the sulfur-infiltrated SCFM (S-SCFM). HR-TEM of the S-SCFM at a higher magnification (Figure 3d) shows the presence of fringe patterns with an interplanar spacing value of 0.2046 nm corresponding to that of crystalline sulfur ( $\alpha$ -S<sub>8</sub>).<sup>71</sup> The inset in Figure 3d also shows the SAED pattern corresponding to S-SCFM. Upon further analysis, the SAED pattern shows spots corresponding to (202), (020) and ( $\bar{1}$ 22) crys-

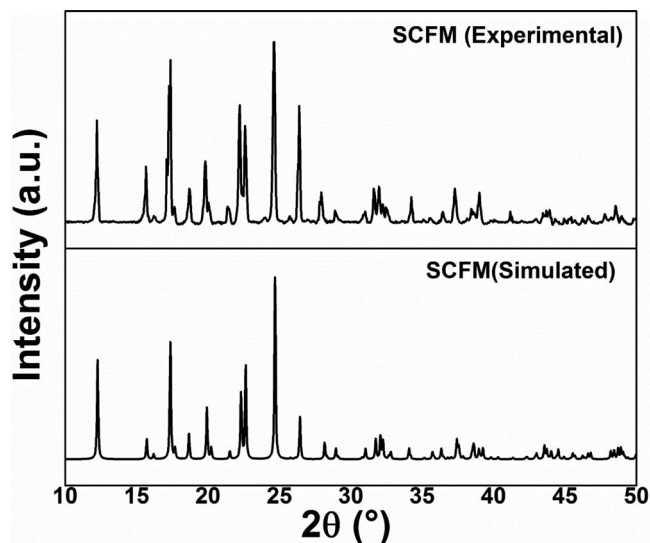


**Figure 2.** XRD patterns of the SCFM structure predicted by simulation and synthesized experimentally showing a positive match.

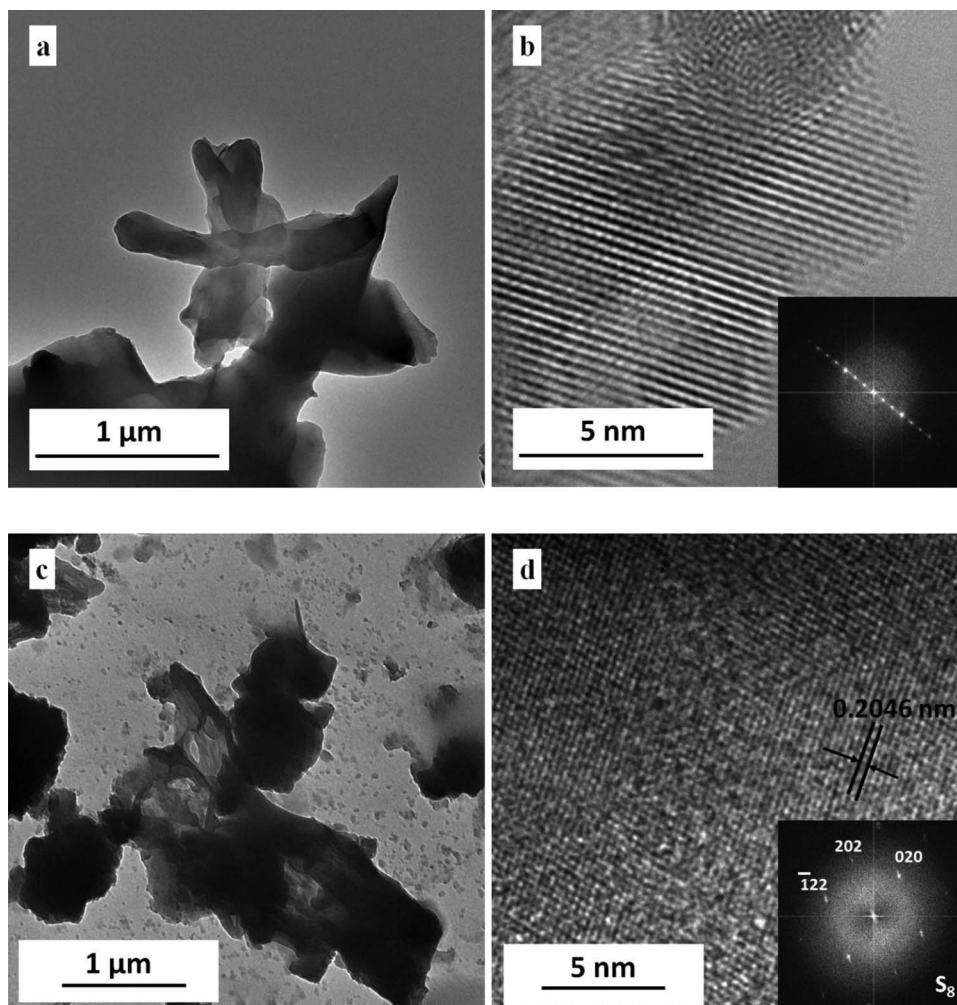


**Figure 3.** a) and b): TEM images of a) Sulfonic acid based CFM derived SCFM at low magnification and b) Sulfonic acid based CFM derived SCFM at high magnification, c) Sulfur incorporated sulfonic acid based CFM derived S-SCFM at low magnification and d) Sulfur incorporated sulfonic acid based CFM derived S-SCFM at high magnification (Inset: SAED pattern of the S-SCFM confirming the presence of sulfur in the S-SCFM).

talline planes of  $\alpha$ -S<sub>8</sub>,<sup>72</sup> thus confirming the presence of crystalline sulfur inside the SCFM. The SEM images of the sulfonic acid derived CFM structures comparing the morphology of the experimentally synthesized SCFM before and following infiltration with sulfur, S-SCFM are shown in Figure S2a-d. Figure S2e and Table S1 represents the EDS (Energy Dispersive X-ray Spectroscopy) pattern and the composition of the SCFM after sulfur infiltration. Table S1 clearly shows that the composition of the experimentally generated sulfur infiltrated S-SCFM is in accordance with the calculated composition, thus confirming complete sulfur infiltration and the presence of  $\sim 70$  wt% sulfur in the S-SCFM following sulfur infiltration.

In order to confirm the presence of sulfur and to understand the nature of the binding between the infiltrated sulfur and the sulfonic acid based CFM derived SCFM, the experimentally synthesized S-SCFM was analyzed using XPS on a background corrected Thermo ESCALAB 250Xi after sulfur infiltration. Figure 4 represents the S2p spectra collected on the sulfur infiltrated into the SCFM, namely, S-SCFM (Figure 4a) compared with that of commercial sulfur (Figure 4b). The characteristic S2p peaks of S<sub>8</sub>, S2p<sub>1/2</sub> and S2p<sub>3/2</sub> were observed at 164.70 eV and 162.90 eV,<sup>63,73–75</sup> respectively for commercial sulfur. On the other hand, the XPS spectra collected on S-SCFM following sulfur infiltration shows S2p peak at 163.20 eV as opposed to the spectra collected on commercial sulfur (S<sub>8</sub>) (which usually occurs at 164.70 eV and 162.90 eV) indicating the absence of free elemental sulfur. The peaks at 170.10 eV and 169.12 eV corresponds to the -Cu-S-O-<sup>76</sup> and -SO<sub>3</sub>-C-<sup>77</sup> bonds that are characteristics of the SCFM.

The S2p<sub>3/2</sub> peak observed at 163.20 eV in the spectra of S-SCFM corresponds to -C-S- bonds as shown by Wagner et al.<sup>78</sup> confirming the chemical binding of sulfur to the CFM derived SCFM arising from the infiltration of sulfur into the chemically derived sulfonic acid based CFM, i.e. SCFM to form the S-SCFM. This binding of the acidic SCFM chemical linkages with the basic sulfur is due to the acidic nature of the synthesized SCFM.<sup>56</sup> This chemical binding of sulfur to the carbon atoms from the sulfonic acid based CFM derived SCFM, along with the nanoporous nature of the SCFM ( $\sim 3.2$  nm from BET (Table I)) would help to immobilize and thereby prevent the dissolution of polysulfide species formed as a result of electrochemical cycling into the electrolyte solution. Further, the SCFM, being derived from sulfonic acid (-SO<sub>3</sub>-) groups, will interact with the basic polysulfides (via Lewis acid-base interaction) that are generated during electrochemical cycling, thereby preventing them from dissolving into the electrolyte. This type of acid – base interaction has been reported in various systems that involves molecular binding of species onto various CFMs.<sup>79,80</sup>

We have also demonstrated complete binding and subsequent trapping of the polysulfide in a carbonate-based MOF (MOF-5) in our previous publication<sup>48</sup>. However, the carbonate-based system showed a very high loss in capacity in the first  $\sim 20$  cycles due to the chemical reaction of sulfur with the -CO<sub>3</sub>- group of the MOF-5 forming sulfate species. The absence of -CO<sub>3</sub>- groups in the currently synthesized sulfonic acid based CFM derived SCFM is evidently expected to reduce this loss in capacity observed in our

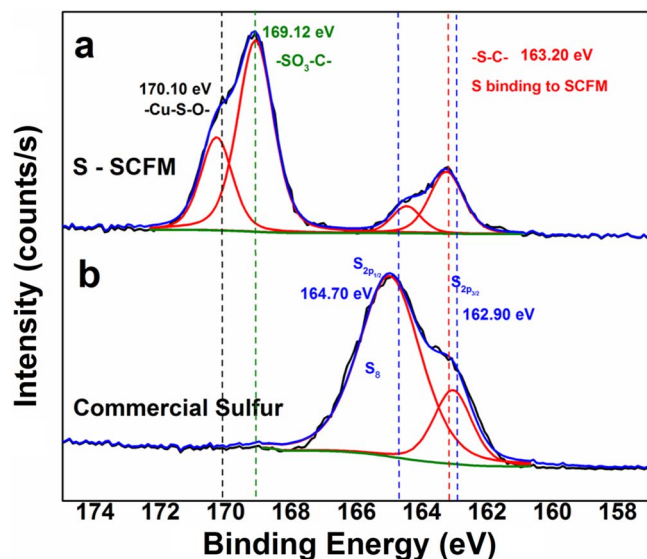


**Figure 4.** XPS S2p Binding Energy profile corresponding to (a) sulfur infiltrated SCFM, S-SCFM and that of (b) commercially obtained Sulfur.

previously reported carbonated based MOFs and lead to improved cycling stability.

Having confirmed the presence of sulfur infiltrated into the sulfonic acid based CFM derived SCFM and the corresponding chemical binding between the synthesized SCFM and infiltrated sulfur, electrochemical charge-discharge cycling was performed on the synthesized sulfur infiltrated SCFM namely, the S-SCFM electrodes to study the effect of this binding on the electrochemical performance of the generated S-SCFM structure. The results of the electrochemical charge-discharge response on the S-SCFM at 0.1C rate ( $\sim 1.5\text{-}2\text{ mgcm}^{-2}$  sulfur loading) and the corresponding rate capability response is shown in Figure 5a. The S-SCFM electrode shows an initial discharge capacity of  $1190\text{ mAh g}^{-1}$  which stabilizes at  $1044\text{ mAh g}^{-1}$  after the 100<sup>th</sup> cycle. Moreover, following cycling of the electrode at 1C rate yielding a capacity of  $669\text{ mAh g}^{-1}$ , the electrode regains the capacity of  $1066\text{ mAh g}^{-1}$  when cycled at 0.1C. Commercial sulfur cathodes on the other hand, when cycled at similar conditions (0.1C rate against lithium metal anode) shows a much lower initial capacity of  $557\text{ mAh/g}$  that fades rapidly to  $81\text{ mAh/g}$  (Figure S3). At the same time, this initial discharge capacity value obtained from the S-SCFM electrode is lower than the initial capacity reported by us in our

previous work using Zn-MOF-5 as sulfur hosts ( $1476\text{ mAh/g}$  at 0.2C rate).<sup>50</sup> It is worthy to note that, in our previous work, 50 wt% sulfur was infiltrated into 50wt.% Zn-MOF-5 and the electrodes had a total sulfur loading of 36 wt%. This could be attributed to the comparatively lower electrical and ionic conductivity of the CMF derived SCFM and S-SCFM as compared to the earlier reported MOF-5 and S-MOF-5 resulting in a lower capacity despite utilizing a higher sulfur loading in the electrodes used in our current S-SCFM cathodes (56 wt%) (see Table S2).

The experimentally synthesized sulfonic acid based CFM derived S-SCFM exhibits electrical conductivity ( $7.64 \pm 0.73 \times 10^{-10}\text{ Scm}^{-1}$ ) and ionic conductivity ( $4.03 \pm 0.12 \times 10^{-10}\text{ Scm}^{-1}$ ) which is an order of magnitude lower than the electrical conductivity ( $1.83 \pm 0.21 \times 10^{-8}\text{ Scm}^{-1}$ ) and ionic conductivity ( $1.37 \pm 0.08 \times 10^{-9}\text{ Scm}^{-1}$ ) of S-MOF-5. The lower ionic and electronic conductivity of the CFM derived S-SCFM could limit the complete utilization of the infiltrated sulfur, hence resulting in specific capacities lower than the theoretical capacity of sulfur ( $1672\text{ mAhg}^{-1}$ ). The voltage versus specific capacity plot of S-SCFM is shown in Figure 5b. The specific capacity plot of the S-SCFM system shows a difference of  $\sim 10\%$  difference between the first cycle charge and discharge capacities, which is accordingly reflected in the coulombic efficiency plot (Figure 5a). This difference is similar to the observations made by Zhao et al.<sup>56</sup> and Zhao et al.<sup>81</sup> in their work on different non-carbonized MOF-based sulfur cathode systems. Both the authors cite the absence of polysulfide dissolution in their respective systems due to Lewis acid-base interaction between the MOF and polysulfides, however, a scientific explanation for this observed difference between the charge and discharge capacity is lacking. In order to additionally prove and provide scientific insights into the observed differences between the first cycle charge and discharge capacities, we have characterized the system extensively by conducting XPS analysis on the separator and the cycled electrodes respectively, the results of which will be discussed in the following sections outlined below.

It should be noted that the sulfonic acid based CFM derived S-SCFM, however, exhibits an exceptionally low fade-rate of 0.0012%/cycle along with good rate-capability and coulombic efficiency ( $\sim 99.9\%$ ). In our previous work reporting the use of carbonate-based S-MOF-5, the capacity was observed to fade rapidly during the first 10 cycles only to stabilize at a capacity of  $609\text{ mAhg}^{-1}$  after 200 cycles with comparable fade rate of  $0.0014\%\text{cycle}^{-1}$ . Table S3 represents a comparison of the performance of all the non-carbonized CFM-based cathode systems reported in the literature thus far. The current work on sulfur infiltrated sulfonic acid based CFM derived S-SCFM system has the highest sulfur contents (56 wt%) in the cathode next to that reported by Zhao et al.<sup>81</sup> in their work on chromium MOF MIL-101 (58.8% wt) and Zheng et al.<sup>56</sup> who describe using

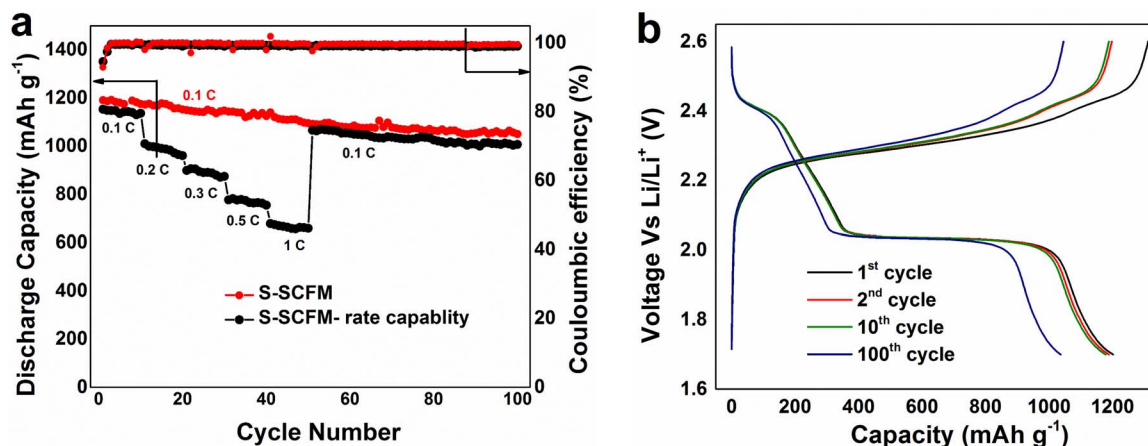


**Figure 5.** a. Electrochemical cycling performance of S-SCFM with coulombic efficiency and b: Specific capacity plots of S-SCFM (The cycling experiment was performed on three batches of S-SCFM samples prepared independently from three batches of CFM derived SCFM samples. The difference in capacity in all the three runs were within  $\pm 5\%$ ).

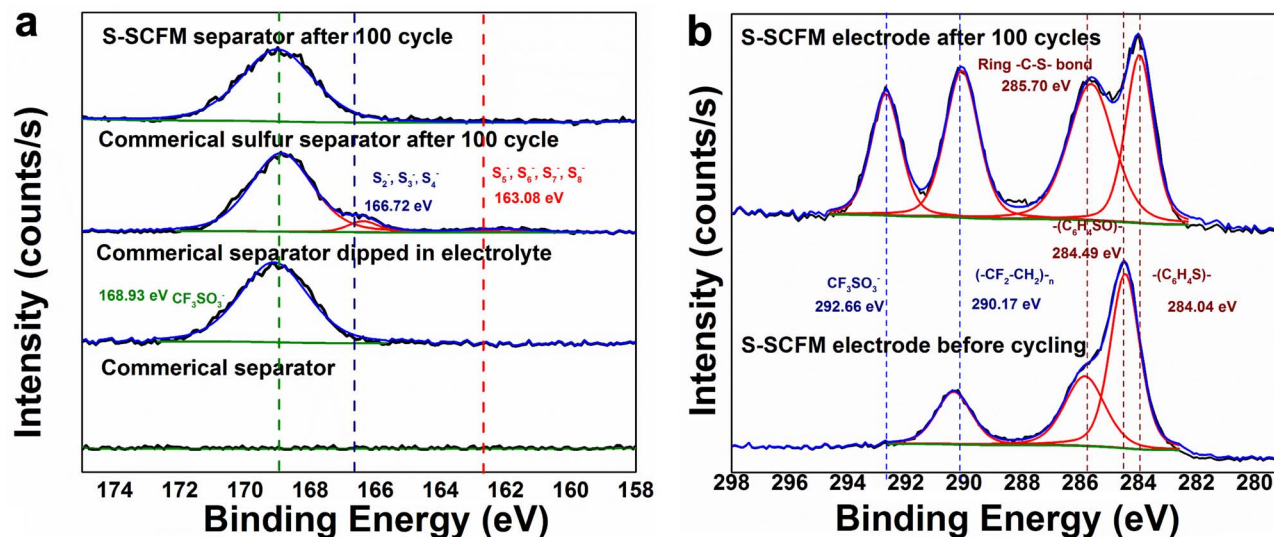


**Figure 6.** a) XPS S2p spectra of commercial separator (Celgard PP), separator soaked in liquid electrolyte, separators cycled with commercial sulfur electrode and sulfonic acid based CFM following sulfur incorporation namely, S-SCFM (after 100 cycles at 0.1 C rate), b) XPS C1s spectra of pristine S-SCFM electrodes before cycling and the electrodes after 100 charge-discharge cycles at 0.1 C rate.

Ni-MOF DUT-23 (60 wt%). The sulfur infiltrated sulfonic acid based CFM derived S-SCFM system used in the work reported herein also exhibits exceptionally high stable discharge capacity of 1044 mAh/g which is the highest value reported in the cited literature thus far to the best of our knowledge. The cycling stability (0.0012%) is also one of the lowest values reported in literature so far. The exceptional electrochemical cycling stability of the sulfur infiltrated sulfonic acid based CFM derived S-SCFM cathodes is due to sulfur binding with the SCFM (confirmed by XPS analysis - Figure 4a) subsequently resulting in effective trapping of polysulfide species inside the nanopores of the sulfonic acid based CFM derived SCFM, namely, S-SCFM architectures.

Confirmation of the complete encapsulation of sulfur and the polysulfide species inside the sulfonic acid based CFM derived sulfur infiltrated SCFM, namely, S-SCFM architectures during the electrochemical charge-discharge cycle, was achieved by conducting XPS. Accordingly, XPS analysis was performed on the separators retrieved from the electrochemically cycled batteries containing the S-SCFM electrodes after 100 cycles and compared with the XPS spectra collected on the separators obtained from electrochemically cycled batteries made from commercially obtained sulfur electrodes. The Celgard separators corresponding to dry and another separator accordingly dipped in the electrolyte were used as the corresponding control samples allowing for suitable comparison. The results of the XPS analysis are accordingly shown in Figure 6a.

In the case of the polypropylene (PP) separator that is dry, no S2p peak was observed before cycling, but in the PP separator dipped in electrolyte, a single peak corresponding to the  $-\text{SO}_3^-$  group from the lithium salt present in the electrolyte (Trifluoro methyl sulfonate lithium salt) is observed at 168.93 eV as seen in Figure 6a.<sup>77</sup> In addition to this peak, the XPS spectra of the separator cycled after 100 cycles with the commercial sulfur electrode shows the characteristic S2p peaks at 166.72 eV and 163.08 eV, arising from the lower and higher order polysulfide species, respectively.<sup>82-85</sup> This validates the fact that the commercial sulfur electrode undergoes polysulfide dissolution into the electrolyte during electrochemical cycling, depositing on the separator. The commercial sulfur cathode, when cycled electrochemically (Figure S3) shows an initial capacity of 557 mAh/g that rapidly fades to 81 mAh/g in the first 100 cycles along with a low coulombic efficiency ( $\sim 80\%$ ). This result confirms and supports our XPS observation clearly indicating the presence of polysulfide dissolution contributing to the characteristic loss in capacity and rapid fade rate observed in electrodes made from commercial sulfur.

However, the separator corresponding to the sulfonic acid based CFM following sulfur infiltration namely, S-SCFM electrode after 100 cycles shows only one S2p peak at 168.93 eV (see Figure 6a) corresponding to the sulfur binding in the  $\text{LiCF}_3\text{SO}_3$  salt present in the electrolyte.<sup>77</sup> The clear absence of polysulfide species related peaks in the sulfonic acid based CFM following sulfur infiltration namely, S-SCFM separator and the lithium counter electrode (see Figure S4) post cycling clearly shows and validates the complete entrapment of the polysulfide species by the S-SCFM architecture. This observation can be attributed to the binding of polysulfide species due to the Lewis acid-base interactions between the synthesized sulfonic acid based CFM derived SCFM and the infiltrated sulfur, as well as the entrapment effect provided by the nanoporous nature of the SCFM as is evident from the TEM (Figure 3) and BET analysis (Table I). Use of a carbonaceous porous matrix<sup>22,23,25,26,39</sup> and conventional carbonate CFMs<sup>56,61</sup> as sulfur hosts reported previously has shown improvement in electrochemical cycling. However, a complete prevention of polysulfide dissolution in the CFM synthesized as outlined herein has not been reported thus far. The unique  $-\text{SO}_3^-$  functional groups present in the precursor used to synthesize the SCFM in the current study, and its chemical inertness to sulfur preventing the formation of any unwanted sulfate species during electrochemical cycling as opposed to our previously published work<sup>50</sup> is clearly responsible for this observed result. Consequently, based on our current studies, it can be stated that the chemically synthesized sulfonic acid based CFM derived SCFM following sulfur incorporation, S-SCFM is not only effective in entrapping the polysulfides but also contributes to elimination of the formation of any metal sulfate species that is responsible for the large first cycle irreversible loss observed and reported by us previously in the carbonate derived CFM structures. Furthermore, the sulfonic acid based CFM derived sulfur infiltrated S-SCFM architecture owing to the presence of the sulfonic acid species leads to exceptional low fade rates of  $\sim 0.0012\%/ \text{cycle}$ .

Following confirmation of no observable and detectable polysulfide species in the separators collected from the battery cycled with S-SCFM electrodes post cycling, the electrodes were further analyzed using XPS both before and after 100 cycles. The C1s spectra collected on the sulfonic acid based CFM following sulfur infiltration, namely, S-SCFM electrodes before cycling and after cycling for 100 cycles are shown in Figure 6b. The S-SCFM electrode before cycling shows a peak at 290.17 eV corresponding to  $(-\text{CF}_2-\text{CH}_2)_n$  bonding from the PVdF binder used in the electrode.<sup>86</sup> The electrode before cycling also shows peaks at 284.49 eV and 285.70 eV corresponding

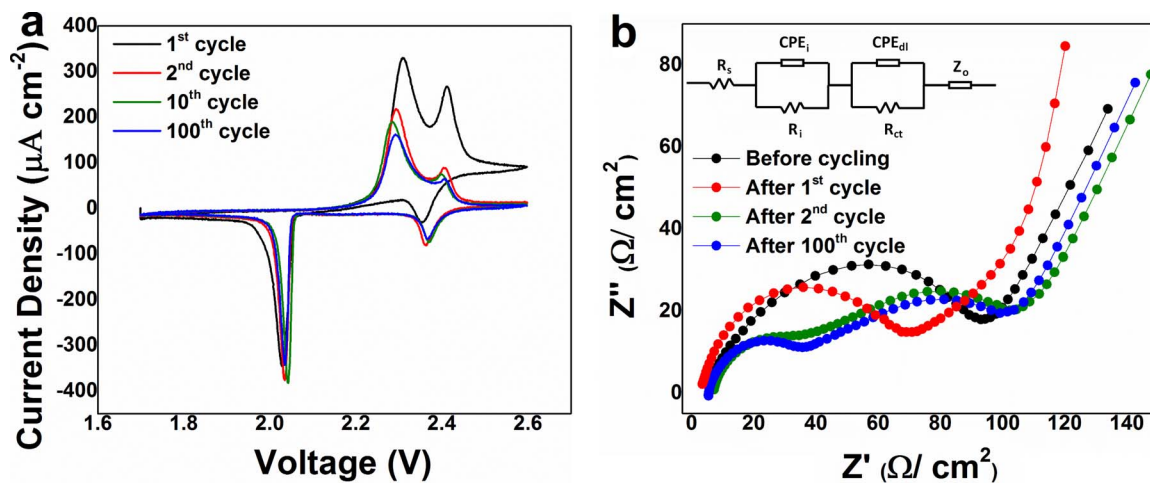


**Figure 7.** a) Cyclic Voltammograms (CV) and b) Electrochemical Impedance Spectroscopy (EIS) plot of S-SCFM at various cycles (scan rate: 0.1mV/s).

to the different types of chemical interactions between the carbon and sulfur in the sulfonic acid based CFM,  $-(C_6H_4SO)-$  bonding<sup>87</sup> and  $-C-S-$  bonding,<sup>88</sup> respectively. The presence of the C-S bond in the XPS spectra validates the observations from Figure 4, that the formation of the sulfur-carbon bonding during infiltration of the sulfur ensures complete retention of the polysulfide species formed within the S-SCFM structure.

The S-SCFM electrode after completing 100 charge-discharge cycles shows the characteristic  $-C-S-$  binding peaks in the sulfur infiltrated S-SCFM electrode as discussed earlier, along with a peak at 292.66 eV corresponding to  $CF_3SO_3^-$  group from the lithium salt ( $LiCF_3SO_3$ ) present in the organic electrolyte used for battery testing. Another additional peak is observed at 284.04 eV that corresponds to the presence of  $-(C_6H_4S)-$ ,<sup>87</sup> which is a slight variation to the binding observed in the electrode before cycling. There is no significant change in the binding state of C1s observed indicating the chemical stability of the S-SCFM upon electrochemical cycling. In our previous work reporting the use of MOF-5 as sulfur host for Li-S battery,<sup>50</sup> we observed peaks corresponding to the reaction of the  $-CO_3-$  groups with sulfur and lithium. However, the absence of any such anomalous peaks in the C1s spectra and the presence of  $-C-S-$  peaks even after 100 charge-discharge cycles is a convincing validation supporting the strong Lewis acid-base interaction of the SCFM with infiltrated sulfur and the polysulfide species.<sup>56</sup>

For gaining further a better understanding of the good cycling stability and low fade-rate observed for the sulfur infiltrated S-SCFM electrodes discussed above, cyclic voltammetry (CV) and electrochemical impedance spectroscopy (EIS) measurements were performed (Figures 7a and 7b). The CVs were performed employing a very slow scan rate of 0.1 mV/s. The two reduction peaks at 2.36 V and 2.03 V correspond to the two discharge plateaus<sup>89</sup> observed in the specific capacity plots (Figure 5b), which results from the transformation processes corresponding to the conversion of the linear  $S_8$  chain to soluble polysulfides  $Li_2S_x$  ( $x = 4-8$ ) and  $Li_2S_4$  to insoluble  $Li_2S$ , respectively.<sup>90</sup> Similarly, the two oxidation peaks observed at 2.40 eV and 2.30 eV corresponds to the two charge plateaus observed in the specific capacity plots (Figure 5b) attributable to the conversion of the insoluble  $Li_2S$  to  $Li_2S_4$  and  $Li_2S_4$  to  $S_8$  via the formation of the ubiquitous soluble polysulfides  $Li_2S_x$  ( $x = 4-8$ ), respectively.<sup>91</sup> It should be noted that there is also no observable change in the peak positions in the charge and discharge peaks (Table S4) over the various cycles indicating lack of any observable irreversible polarization occurring in the assembled electrode suggesting the reversible nature of the CFM derived S-SCFM system. However, there is indeed a change in the peak height observed between the first and second cycle. This change in the peak height has been reported in the literature as well and is believed to be due to the formation of the solid electrolyte inter-

terphase (SEI) as is well-known in all electrochemical systems and is also discussed below.<sup>92</sup>

Electrochemical Impedance Spectroscopy (EIS) measurement was employed to understand further the behavior observed in the CV experiments. Figure 7b represents the results of the EIS analysis conducted on the S-SCFM system (before and after the 1<sup>st</sup>, 2<sup>nd</sup> and 100<sup>th</sup> cycles) between a frequency range of 0.01Hz to 100,000Hz at an applied amplitude of 10mV at the open circuit potential. The EIS spectra were fitted to the Randles circuit model (Figure 7b inset) comprised of two semicircles in the low frequency regime corresponding to the charge transfer reaction ( $R_{ct}$  and  $CPE_{ct}$ )<sup>93</sup> with the medium frequency region corresponding to the resistances and capacitances at the interface ( $R_i$  and  $CPE_{dl}$ ).<sup>94</sup> Additionally, the characteristic sloping line in the very low frequency region is attributed to the Warburg impedance ( $Z_w$ ), the values of which are tabulated in Table S5. Before cycling, the initial resistance is very high at 107.2  $\Omega$  due to the relatively poor conductivity of the S-SCFM (as discussed in Table S2). During the first discharge process, lithium reacts with sulfur to form polysulfides that exhibit higher conductivity. Hence, there is a decrease in the charge transfer resistance,  $R_{ct}$  to 89.5 $\Omega$ . These results are in accordance with the results reported in the literature in experiments conducted on CFM-based systems.<sup>56</sup> However, after the second cycle there is a considerable decrease in the  $R_{ct}$  (70.1 $\Omega$ ), which almost remains constant up until after 100 cycles (68.8 $\Omega$ ). The change in the value of  $R_{ct}$  between the first discharge and the second discharge also hints at the formation of a SEI layer on the electrode surface, which requires further chemical characterization as is discussed below.

For further explaining the difference observed in the peak heights between the first and the second cycle observed in the CV (Figure 7a), XPS analysis was carried out on the pristine uncycled sulfonic acid based CFM derived sulfur infiltrated S-SCFM electrode as well as on the electrode after the first discharge cycle. A comparison of the S2p spectra is shown in Figure 8. The S2p spectra of the S-SCFM electrode before cycling shows peaks at 170.10 eV and 169.12 eV corresponding to the  $-Cu-S-O-$ <sup>76</sup> and  $-SO_3-C-$ <sup>77</sup> groups, respectively, both of which are characteristic of the SCFM. In addition, a peak at 163.20 eV is observed in the spectra of the S-SCFM corresponding to  $-C-S-$  and  $-S-O-$  bonds<sup>78</sup> formed due to the chemical interaction of sulfur with the carbon in the SCFM as discussed earlier. The S2p spectra of the S-SCFM after the 1<sup>st</sup> charge-discharge cycle shows all the peaks observed before cycling, along with a new peak at 166.76 eV corresponding to  $Li_2SO_3$ .<sup>95,96</sup> This peak at 166.76 is likely arising from the decomposition of the liquid electrolyte containing  $LiCF_3SO_3$  at the electrode surface to form the characteristic SEI. This SEI formed during the initial cycle confirms the observed change in peak height seen in the CV and the characteristic EIS signature discussed above. The formation of this SEI layer is however, expected to stabilize the electrode.

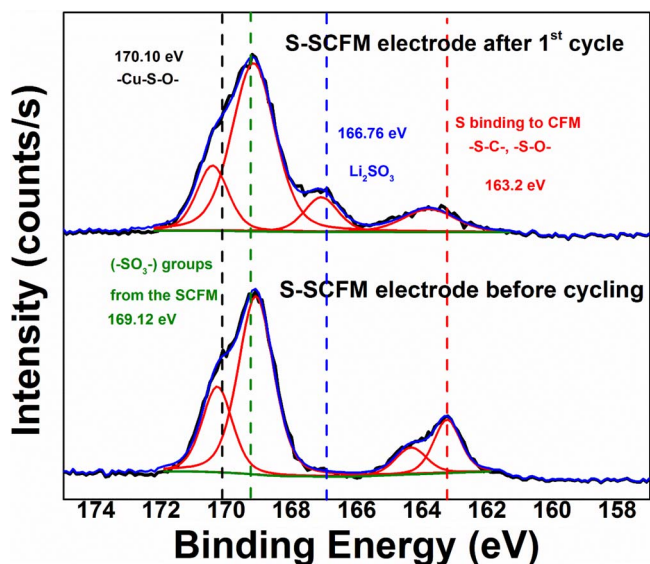


**Figure 8.** XPS S2p spectra of slurry coated electrodes of the CFM derived S-SCFM-before and after 1<sup>st</sup> cycle (0.1 C rate).

Formation and stabilization of the electrode indeed explains the absence of a significant change in the peak height in the CV (Figure 7a) collected on the electrode following subsequent cycles after the 1<sup>st</sup> cycle.

From the results of our previous study on carbonate-based CFM host for sulfur, it is indeed evident that the presence of electrochemically unstable carbonate groups in the CFM resulted in the formation of metal sulfate complexes during the initial charge-discharge cycles. These sulfate complexes lead to irreversible loss in capacity despite its ability to successfully prevent polysulfide species from dissolving into the electrolyte.<sup>50</sup> Hence, by generating a CFM architecture as outlined herein using a sulfonic acid-based CFM (SCFM), this problem of the initial capacity loss that we previously observed in our carbonate derived CFM is indeed overcome in the present study. The results discussed in this work herein further suggests that the use of this sulfonic acid based CFM derived from a non-carbonate species containing CFM could ably function as potential hosts for sulfur thus serving as a promising pathway toward the fabrication of stable and reversible Li-S battery electrodes exhibiting better capacity and exceptional stability. The results of this study described herein indeed could serve to provide better insights into the designing of next generation complex framework materials (CFM) type CFM based sulfur hosts functioning as effective architectures for entrapment of polysulfide species leading to high energy density Li-S batteries. The efficient polysulfide trapping as evinced from the results here combined with the elimination of the metal sulfate species provides an elegant pathway for further modification of the system to demonstrate the creation of the next generation electrodes with high sulfur loading while still demonstrating the excellent capacity retention. The results of the current study will nevertheless provide insights for these studies to be conducted in the near future.

### Conclusions

A sulfonic acid-based complex framework material (CFM), termed as SCFM was effectively synthesized at room temperature and infiltrated with sulfur using a vapor-phase infiltration technique to form S-SCFM. The S-SCFM electrode was then tested as a cathode for Li-S batteries. The S-SCFM electrode demonstrated a high initial capacity of 1190 mAhg<sup>-1</sup>, with stable capacity of 1044 mAhg<sup>-1</sup> for up to 100 cycles when cycled at 0.1C rate while also exhibiting reversible capacity of 669 mAhg<sup>-1</sup> at 1C rate. The electrode regains the capacity of 1066 mAhg<sup>-1</sup> when cycled back at 0.1C. The S-SCFM also exhibited

good cycling stability along with a low fade rate of  $\sim 0.0012\%$ /cycle. The higher discharge capacity along with impressive cycling stability makes the sulfonic acid based CFM namely, SCFM an appealing sulfur host to form S-SCFM structures serving as effective operational electrodes for Li-S batteries. XPS analysis of the S-SCFM separators post-cycling shows the absence of any polysulfide species, which is attributed to the binding of the infiltrated sulfur with the carbon from the SCFM backbone and the ability of the SCFM to interactively bind polysulfide species through the characteristic Lewis acid-Lewis base interactions. These interactions accordingly, prevent the polysulfide species from dissolving and diffusing into the electrolyte during electrochemically cycling. The study also provides insights into stabilizing and entrapping the polysulfide species using the porous, non-carbonized sulfonic acid based polymeric complex framework material (CFM) acting as effective sulfur hosts. The results of this study demonstrate the promise of designing and developing new sulfonic acid, based CFM derived SCFM serving as effective and efficient sulfur hosts with potentially maintaining higher sulfur loadings that are capable of adroitly preventing polysulfide dissolution. At the same time, these systems will likely demonstrate the ability to deliver a high energy density in the range of  $\sim 500$  Whkg<sup>-1</sup> needed and desired for next generation Li-S batteries for electric vehicle technology applications.

### Acknowledgments

This research was supported by the Department of Energy (DOE) grant OVT-DE-EE0006825, DE-EE0007797, and DE-EE0008199. The authors also acknowledge the Edward R. Weidlein Chair Professorship Funds, the Center for Complex Engineered Multifunctional Materials (CCEMM) and NSF-CBET 1511390 for supporting the research while also providing the required equipment for characterization as needed for this study. The authors also further acknowledge Dr. Joel Gillespie, PPG Materials Characterization Laboratory (Department of Chemistry, University of Pittsburgh) for providing access to the use of XPS instrumentation. Finally, the authors acknowledge the help of Karthikeyan Saravanan, Dr. John Keith and Brian Day (Department of Chemical Engineering, University of Pittsburgh) for their help in simulating the XRD pattern from CIF (Crystallographic Information File) information as well as generation of the schematic plots of the SCFM and S-SCFM structures.

### ORCID

Prashant N. Kumta  <https://orcid.org/0000-0003-1227-1249>

### References

- N. Nitta, F. Wu, J. T. Lee, and G. Yushin, *Materials Today*, **18**, 252 (2015).
- J. Janek and W. G. Zeier, *Nat. Energy*, **1**, 16141 (2016).
- V. Etacheri, R. Marom, R. Elazari, G. Salitra, and D. Aurbach, *Energy & Environmental Science*, **4**, 3243 (2011).
- J. B. Goodenough and Y. Kim, *Chem. Mater.*, **22**, 587 (2010).
- P. G. Bruce, B. Scrosati, and J. M. Tarascon, *Angewandte Chemie*, International Edition, **47**, 2930 (2008).
- S.-Y. Chung, J. T. Bloking, and Y.-M. Chiang, *Nature Materials*, **1**, 123 (2002).
- J. Li, Z. Du, R. E. Ruther, S. J. AN, L. A. David, K. Hays, M. Wood, N. D. Phillip, Y. Sheng, C. Mao, S. Kalnaus, C. Daniel, and D. L. Wood, *JOM*, **69**, 1484 (2017).
- A. K. Padhi, K. S. Nanjundaswamy, and J. B. Goodenough, *Journal of The Electrochemical Society*, **144**, 1188 (1997).
- A. Yamada, S. C. Chung, and K. Hinokuma, *Journal of The Electrochemical Society*, **148**, A224 (2001).
- B. Scrosati, *Electrochimica Acta*, **45**, 2461 (2000).
- C. K. Chan, H. Peng, G. Liu, K. McIlwrath, X. F. Zhang, R. A. Huggins, and Y. Cui, *Nature Nanotechnology*, **3**, 31 (2007).
- P. G. Bruce, S. A. Freunberger, L. J. Hardwick, and J.-M. Tarascon, *Nat Mater*, **11**, 19 (2012).
- J. Kim, D. J. Lee, H. G. Jung, Y. K. Sun, J. Hassoun, and B. Scrosati, *Advanced Functional Materials*, **23**, 1076 (2013).
- A. Fotouhi, D. J. Auger, L. O'Neill, T. Cleaver, and S. Walus, *Energies*, **10**, 1937 (2017).
- G. Berckmans, M. Messagie, J. Smekens, N. Omar, L. Vanhaverbeke, and J. Van Mierlo, *Energies*, **10**, 1314 (2017).

16. H. D. Holland and K. K. Turekian, *Geochemistry of earth surface systems: A derivative of the treatise on geochemistry*, Academic Press, 2010.
17. Q. Pang, X. Liang, C. Y. Kwok, and L. F. Nazar, *Nat. Energy*, **1**, 16132 (2016).
18. P. J. Hanumantha, B. Gattu, O. Velikokhatnyi, M. K. Datta, S. S. Damle, and P. N. Kumta, *Journal of The Electrochemical Society*, **161**, A1173 (2014).
19. Y. V. Mikhaylik and J. R. Akridge, *Journal of The Electrochemical Society*, **151**, A1969 (2004).
20. C. Zu and A. Manthiram, *J. Phys. Chem. Lett.*, **5**, 2522 (2014).
21. S. Evers, T. Yim, and L. F. Nazar, *The Journal of Physical Chemistry C*, **116**, 19653 (2012).
22. B. Ding, C. Yuan, L. Shen, G. Xu, P. Nie, and X. Zhang, *Chemistry – A European Journal*, **19**, 1013 (2013).
23. Z. Gong, Q. Wu, F. Wang, X. Li, X. Fan, H. Yang, and Z. Luo, *RSC Advances*, **6**, 37443 (2016).
24. G. He, X. Ji, and L. Nazar, *Energy & Environmental Science*, **4**, 2878 (2011).
25. D. Li, F. Han, S. Wang, F. Cheng, Q. Sun, and W.-C. Li, *ACS Applied Materials & Interfaces*, **8**, 2208 (2013).
26. X. Liang, Z. Wen, Y. Liu, H. Zhang, L. Huang, and J. Jin, *Journal of Power Sources*, **196**, 3655 (2011).
27. Z. Yuan, H. J. Peng, J. Q. Huang, X. Y. Liu, D. W. Wang, X. B. Cheng, and Q. Zhang, *Adv. Funct. Mater.*, **24**, 6105 (2014).
28. L. L. Kong, Z. Zhang, Y. Z. Zhang, S. Liu, G. R. Li, and X. P. Gao, *ACS Appl. Mater. Interfaces*, **8**, 31684 (2016).
29. X. Ji, D. Y. Liu, D. G. Prendiville, Y. Zhang, X. Liu, and G. D. Stucky, *Nano Today*, **7**, 10 (2012).
30. N. Ding, L. Zhou, C. Zhou, D. Geng, J. Yang, S. W. Chien, Z. Liu, M. F. Ng, A. Yu, and T. S. A. Hor, *Sci. Rep.*, **6**, 33154 (2016).
31. S. Xiong, K. Xie, Y. Diao, and X. Hong, *Electrochim. Acta*, **83**, 78 (2012).
32. S. S. Zhang, *Electrochim. Acta*, **70**, 344 (2012).
33. M.-S. Song, S.-C. Han, H.-S. Kim, J.-H. Kim, K.-T. Kim, Y.-M. Kang, H.-J. Ahn, S. X. Dou, and J.-Y. Lee, *Journal of The Electrochemical Society*, **151**, A791 (2004).
34. Y. Choi, B. Jung, D. Lee, J. Jeong, K. Kim, H. Ahn, K. Cho, and H. Gu, *Physica Scripta*, **2007**, 62 (2007).
35. X. Ji, S. Evers, R. Black, and L. F. Nazar, *Nature communications*, **2**, 325 (2011).
36. C. Jin, O. Sheng, J. Luo, H. Yuan, C. Fang, W. Zhang, H. Huang, Y. Gan, Y. Xia, and C. Liang, *Nano Energy*, **37**, 177 (2017).
37. Q. Li, S. Zhu, and Y. Lu, *Adv. Funct. Mater.*, **27**, 1606422 (2017).
38. Y. Li, K. W. Wong, and K. M. Ng, *Chem. Commun.*, **52**, 4369 (2016).
39. J. Jin, Z. Wen, G. Ma, Y. Lu, and K. Rui, *Solid State Ionics*, **262**, 170 (2014).
40. X. Li, Y. Cao, W. Qi, L. V. Saraf, J. Xiao, Z. Nie, J. Mietek, J.-G. Zhang, B. Schwenzer, and J. Liu, *Journal of Materials Chemistry*, **21**, 16603 (2011).
41. S.-R. Chen, Y.-P. Zhai, G.-L. Xu, Y.-X. Jiang, D.-Y. Zhao, J.-T. Li, L. Hu, and S.-G. Sun, *Electrochimica Acta*, **56**, 9549 (2011).
42. J. Schuster, G. He, B. Mandlmeier, T. Yim, K. T. Lee, T. Bein, and L. F. Nazar, *Angewandte Chemie International Edition*, **51**, 3591 (2012).
43. R. Elazari, G. Salitra, A. Garsuch, A. Panchenko, and D. Aurbach, *Advanced Materials*, **23**, 5641 (2011).
44. S.-C. Han, M.-S. Song, H. Lee, H.-S. Kim, H.-J. Ahn, and J.-Y. Lee, *Journal of The Electrochemical Society*, **150**, A889 (2003).
45. W. K. Shin, A. G. Kannan, and D. W. Kim, *ACS Appl. Mater. Interfaces*, **7**, 23700 (2015).
46. Z. Wei Seh, W. Li, J. J. Cha, G. Zheng, Y. Yang, M. T. McDowell, P.-C. Hsu, and Y. Cui, *Nature communications*, **4**, 1331 (2013).
47. X. Liang, C. Y. Kwok, F. Lodi-Marzano, Q. Pang, M. Cuisinier, H. Huang, C. J. Hart, D. Houtarde, K. Kaup, H. Sommer, T. Brezesinski, J. Janek, and L. F. Nazar, *Advanced Energy Materials*, **6**, 1501636-n/a (2016).
48. G. Zhou, H. Tian, Y. Jin, X. Tao, B. Liu, R. Zhang, Z. W. Seh, D. Zhuo, Y. Liu, and J. Sun, *Proc. Natl. Acad. Sci. U. S. A.*, **114**, 840 (2017).
49. C. Yan, X. B. Cheng, C. Z. Zhao, J. Q. Huang, S. T. Yang, and Q. Zhang, *J. Power Sources*, **327**, 212 (2016).
50. P. M. Shanthi, P. J. Hanumantha, B. Gattu, M. Sweeney, M. K. Datta, and P. N. Kumta, *Electrochimica Acta*, **229**, 208 (2017).
51. H. Park and D. J. Siegel, *Chemistry of Materials*, **29**, 4932 (2017).
52. F. Li, X. Zhang, X. Liu, and M. Zhao, *ACS Applied Materials & Interfaces*, (2018).
53. K. Xi, S. Cao, X. Peng, C. Ducati, R. Vasant Kumar, and A. K. Cheetham, *Chemical Communications*, **49**, 2192 (2013).
54. X.-J. Hong, T.-X. Tan, Y.-K. Guo, X.-Y. Tang, J.-Y. Wang, W. Qin, and Y.-P. Cai, *Nanoscale*, **10**, 2774 (2018).
55. G. Xu, B. Ding, L. Shen, P. Nie, J. Han, and X. Zhang, *Journal of Materials Chemistry A*, **1**, 4490 (2013).
56. J. Zheng, J. Tian, D. Wu, M. Gu, W. Xu, C. Wang, F. Gao, M. H. Engelhard, J.-G. Zhang, J. Liu, and J. Xiao, *Nano Letters*, **14**, 2345 (2014).
57. W. Bao, Z. Zhang, C. Zhou, Y. Lai, and J. Li, *Journal of Power Sources*, **248**, 570 (2014).
58. W. Bao, Z. Zhang, Y. Qu, C. Zhou, X. Wang, and J. Li, *Journal of Alloys and Compounds*, **582**, 334 (2014).
59. H. B. Wu, S. Wei, L. Zhang, R. Xu, H. H. Hng, and X. W. Lou, *Chemistry – A European Journal*, **19**, 10804 (2013).
60. X. Li, Q. Sun, J. Liu, B. Xiao, R. Li, and X. Sun, *Journal of Power Sources*, **302**, 174 (2016).
61. Z. Wang, X. Li, Y. Cui, Y. Yang, H. Pan, Z. Wang, C. Wu, B. Chen, and G. Qian, *Crystal Growth & Design*, **13**, 5116 (2013).
62. A. Mietrach, T. W. T. Muesmann, J. Christoffers, and M. S. Wickleder, *European Journal of Inorganic Chemistry*, **2009**, 5328 (2009).
63. T. Fujimori, A. Morelos-Gómez, Z. Zhu, H. Muramatsu, R. Futamura, K. Urita, M. Terrones, T. Hayashi, M. Endo, S. Young Hong, Y. Chul Choi, D. Tománek, and K. Kaneko, *Nat Commun*, **4** (2013).
64. R. Chen, T. Zhao, T. Tian, S. Cao, P. R. Coxon, K. Xi, D. Fairen-Jimenez, R. Vasant Kumar, and A. K. Cheetham, *APL Materials*, **2**, 124109 (2014).
65. N. Jayaprakash, J. Shen, S. S. Moganty, A. Corona, and L. A. Archer, *Angewandte Chemie*, **123**, 6026 (2011).
66. E. L. First and C. A. Floudas, *Microporous and Mesoporous Materials*, **165**, 32 (2013).
67. U. Ravon, M. E. Domine, C. Gaudillere, A. Desmartin-Chomel, and D. Farrusseng, *New Journal of Chemistry*, **32**, 937 (2008).
68. J. Ren, D. E. C. Rogers, T. Segakweng, H. W. Langmi, B. C. North, M. Mathe, and D. Bessarabov, *International Journal of Materials Research*, **105**, 89 (2013).
69. Y. Li, H.-M. Guan, T.-S. Chung, and S. Kulprathipanja, *Journal of Membrane Science*, **275**, 17 (2006).
70. S. Kwon and J. J. Pignatello, *Environmental Science & Technology*, **39**, 7932 (2005).
71. T. Fujimori, A. Morelos-Gómez, Z. Zhu, H. Muramatsu, R. Futamura, K. Urita, M. Terrones, T. Hayashi, M. Endo, and S. Y. Hong, *Nature communications*, **4**, 2162 (2013).
72. Y. Zhang, Z. Gao, N. Song, and X. Li, *Electrochimica Acta*, **222**, 1257 (2016).
73. X.-R. Yu, F. Liu, Z.-Y. Wang, and Y. Chen, *Journal of Electron Spectroscopy and Related Phenomena*, **50**, 159 (1990).
74. G. Hollinger, P. Kumurdjian, J. M. Mackowski, P. Pertosa, L. Porte, and T. M. Duc, *Journal of Electron Spectroscopy and Related Phenomena*, **5**, 237 (1974).
75. J. M. Thomas, I. Adams, R. H. Williams, and M. Barber, *Journal of the Chemical Society, Faraday Transactions 2: Molecular and Chemical Physics*, **68**, 755 (1972).
76. E. Z. Kurmaev, V. V. Fedorenko, V. R. Galakhov, S. Bartkowski, S. Uhlbrock, M. Neumann, P. R. Slater, C. Greaves, and Y. Miyazaki, *Journal of Superconductivity*, **9**, 97 (1996).
77. B. J. Lindberg, K. Hamrin, G. Johansson, U. Gelius, A. Fahlman, C. Nordling, and K. Siegbahn, *Physica Scripta*, **1**, 286 (1970).
78. C. D. Wagner and J. A. Taylor, *Journal of Electron Spectroscopy and Related Phenomena*, **28**, 211 (1982).
79. A. S. Munch and F. O. R. L. Mertens, *CrystEngComm*, **17**, 438 (2015).
80. Z. Akimbekov, D. Wu, C. K. Brozek, M. Dinca, and A. Navrotsky, *Physical Chemistry Chemical Physics*, **18**, 1158 (2016).
81. Z. Zhao, S. Wang, R. Liang, Z. Li, Z. Shi, and G. Chen, *Journal of Materials Chemistry A*, **2**, 13509 (2014).
82. X. Liang, C. Hart, Q. Pang, A. Garsuch, T. Weiss, and L. F. Nazar, *Nat Commun*, **6** (2015).
83. C. Zu, Y. Fu, and A. Manthiram, *Journal of Materials Chemistry A*, **1**, 10362 (2013).
84. Y.-S. Su, Y. Fu, T. Cochell, and A. Manthiram, *Nat Commun*, **4** (2013).
85. C. Zu, N. Azimi, Z. Zhang, and A. Manthiram, *Journal of Materials Chemistry A*, **3**, 14864 (2015).
86. S. Dapoz, N. Betz, M.-J. Guittet, and A. Le Moël, *Nuclear Instruments and Methods in Physics Research Section B: Beam Interactions with Materials and Atoms*, **105**, 120 (1995).
87. J. Riga, P. Snaeuwaert, A. De Pryck, R. Lazzaroni, J. P. Boutique, J. J. Verbist, J. L. Brédas, J. M. André, and C. Taliani, *Synthetic Metals*, **21**, 223 (1987).
88. D. R. Huntley, *The Journal of Physical Chemistry*, **96**, 4550 (1992).
89. Z. Li, L. Yuan, Z. Yi, Y. Liu, Y. Xin, Z. Zhang, and Y. Huang, *Nanoscale*, **6**, 1653 (2014).
90. M.-K. Song, E. J. Cairns, and Y. Zhang, *Nanoscale*, **5**, 2186 (2013).
91. J.-Q. Huang, Q. Zhang, H.-J. Peng, X.-Y. Liu, W.-Z. Qian, and F. Wei, *Energy & Environmental Science*, **7**, 347 (2014).
92. Y. Lu, X. Li, J. Liang, L. Hu, Y. Zhu, and Y. Qian, *Nanoscale*, **8**, 17616 (2016).
93. S. S. Zhang, *Journal of Power Sources*, **231**, 153 (2013).
94. S. S. Zhang and D. T. Tran, *Journal of Power Sources*, **211**, 169 (2012).
95. W. Yao, Z. Zhang, J. Gao, J. Li, J. Xu, Z. Wang, and Y. Yang, *Energy & Environmental Science*, **2**, 1102 (2009).
96. X. Li, Z. Yin, X. Li, and C. Wang, *Ionics*, **20**, 795 (2014).